

# Separating Homogeneous and Inhomogeneous Line Widths of Heavy- and Light-Hole Excitons in Weakly Disordered Semiconductor Quantum Wells

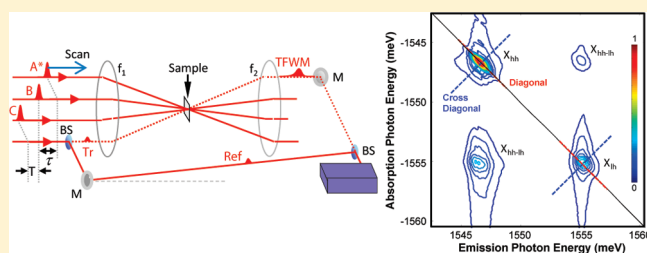
Alan D. Bristow,<sup>†,||</sup> Tianhao Zhang,<sup>†,‡,⊥</sup> Mark E. Siemens,<sup>†,||</sup> Steven T. Cundiff,<sup>\*,†,‡</sup> and R. P. Mirin<sup>§</sup>

<sup>†</sup>JILA, University of Colorado and National Institute of Standards and Technology, Boulder, Colorado 80309-0440, United States

<sup>‡</sup>Department of Physics, University of Colorado, Boulder, Colorado 80309-0390, United States

<sup>§</sup>National Institute of Standards and Technology, Boulder, Colorado 80305, United States

**ABSTRACT:** Optical two-dimensional Fourier-transform spectroscopy is used to study the heavy- and light-hole excitonic resonances in weakly disordered GaAs quantum wells. Homogeneous and inhomogeneous broadening contribute differently to the two-dimensional resonance line shapes, allowing separation of homogeneous and inhomogeneous line widths. The heavy-hole exciton exhibits more inhomogeneous than homogeneous broadening, whereas the light-hole exciton shows the reverse. This situation occurs because of the interplay between the length scale of the disorder and the exciton Bohr radius, which affects the exciton localization and scattering. Utilizing this separation of line widths, excitation-density-dependent measurements reveal that many-body interactions alter the homogeneous dephasing, while disorder-induced dephasing is unchanged.



## INTRODUCTION

Semiconductor quantum wells (QWs) are nanometer-scale buried epitaxial films that confine electron and hole wave functions in one dimension, leaving the electrons and holes freedom to move in the other two dimensions. At low temperatures, optical excitation can lead to the formation of bound electron–hole pairs, known as Wannier–Mott excitons. Even in high-quality QW samples, excitons experience structural disorder through changes in the confinement potential. In general, the disorder can occur because of monolayer fluctuations of the QW thickness (in all cases)<sup>1</sup> and/or through alloy fluctuations (in ternary QWs).<sup>2,3</sup> Disorder leads to inhomogeneous broadening of the excitonic spectral line. Unfortunately, one-dimensional linear optical spectra cannot unambiguously differentiate between homogeneous and inhomogeneous broadening, especially in the weakly disordered limit, that is, when the homogeneous and inhomogeneous line widths are similar.

Ultrafast nonlinear optical experiments have attempted to measure the line widths of excitons in semiconductor QWs with better accuracy than linear spectroscopy.<sup>4,5</sup> However, pump–probe, spectral hole-burning, and transient four-wave mixing (TFWM) all have limited capability of separating the homogeneous and inhomogeneous contributions. Most promising are time-resolved TFWM measurements that give rise to a photon echo for inhomogeneously broadened resonances. In these measurements, the temporal width of the echo is proportional to the inhomogeneous line width. Photon echoes are poorly defined<sup>6</sup> when beats occur between multiple (simultaneously excited) resonances.<sup>7</sup> Moreover, coherent contributions to the TFWM strongly depend on excitation conditions because the

coherent optical response is dominated by excitation-induced many-body interactions.<sup>8–19</sup> Many-body interactions can suppress or enhance the TFWM signal, even in the absence of disorder. However, disorder also modifies the TFWM signal and exhibits strong polarization dependence in both time-integrated and time-resolved measurements.<sup>20,21</sup> Experiments have shown coherent contributions to the disorder-induced dephasing through excitation pathways for the exciton<sup>22</sup> and biexciton<sup>23,24</sup> (bound excitonic molecules). As an alternative to nonlinear approaches, time and angularly resolving the secondary emission has been used to separate inhomogeneous and homogeneous broadening.<sup>25</sup>

The complicated coherent optical response of semiconductor QWs is ideal for study with optical two-dimensional Fourier-transform (2DFT) spectroscopy,<sup>26–29</sup> which is a sophisticated coherent spectroscopic technique that is based on, and supersedes, TFWM. Multidimensional Fourier transform spectroscopy was originally developed in nuclear magnetic resonance.<sup>30</sup> Implementing 2DFT spectroscopy using lasers was first proposed by Tanimura and Mukamel using a Raman excitation scheme to probe molecular vibrations.<sup>31</sup> It is now extensively used in the infrared to probe molecular vibrations.<sup>28</sup> Optical 2DFT spectroscopy uses a multipulsed excitation and detection scheme that provides several time delays from which to build a

**Special Issue:** Shaul Mukamel Festschrift

**Received:** September 30, 2010

**Revised:** January 3, 2011

**Published:** March 09, 2011

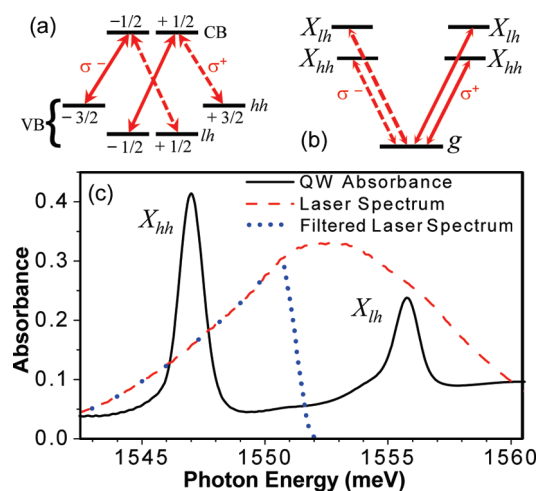


**Figure 1.** (a) Magnetic sublevel diagram for electronic states of a QW and (b) the corresponding center-of-mass excitonic states. Transitions for  $\sigma^+$  and  $\sigma^-$  polarization are differentiated by solid and dashed lines respectively. (c) Linear absorbance (solid line) of the GaAs QW sample, the full laser spectrum (red dashed) and the laser spectrum filtered to excite only the  $X_{lh}$  (blue dots).

multidimensional phase-correlated time map of the coherent response. A 2DFT is performed on the acquired data with respect to two time axes, spreading the information onto a two-dimensional absorption-emission frequency (or photon energy) map. This process separates the intra-action, that is, due to a single resonance, and interaction, that is, due to more than one resonance, spectral contributions of the third-order nonlinear response. To date, GaAs QWs have been studied with 2DFT spectroscopy to separate the single-quantum<sup>32,33</sup> and two-quantum<sup>34–36</sup> many-body interactions, to isolate the upper-state Raman-like coherences,<sup>37</sup> and to extract polarization-dependent dephasing of various contributions to the coherent response.<sup>38,39</sup> These studies include the phase-resolved response,<sup>40</sup> which contains further information about the many-body interactions.<sup>33,36,38,39</sup> 2DFT spectra of single quantum dots have been obtained using an approach based on heterodyne spectral interferometry.<sup>41</sup> In addition to semiconductors, optical 2DFT spectroscopy has been used to study electronic excitations in molecules<sup>27</sup> including photosynthetic complexes<sup>42</sup> where it has provided evidence that the quantum coherence plays a role in light harvesting.<sup>43</sup>

Optical 2DFT spectroscopy can also separate the homogeneous and inhomogeneous line widths for each (nonoverlapping) resonance.<sup>6</sup> This capability is best demonstrated by considering the linear absorbance spectrum of a GaAs QW. The quantum confinement splits the valence bands (VB) into heavy-hole (hh) and light-hole (lh) bands, as shown in Figure 1a (sample details are given later). Excitation from the VB to conduction band (CB) produces two different species of excitons ( $X_{hh}$  and  $X_{lh}$ ) with different electron and hole spin configurations; see Figure 1b. From the linear absorbance spectrum in Figure 1c, the full width at half-maxima are 1.15 meV for the  $X_{hh}$  and 1.22 meV for the  $X_{lh}$ . Solely on the basis of the similarity of the two line widths, it might be expected that both resonances are broadened by the same mechanisms. However, we will show results acquired from 2DFT spectroscopy that contradict this expectation. The two-dimensional line shape of the  $X_{hh}$  is diagonally elongated, which typifies an inhomogeneously broadened resonance.<sup>39</sup> In contrast, the  $X_{lh}$  is mostly “star” shaped, which is indicative of a homogeneously broadened resonance.

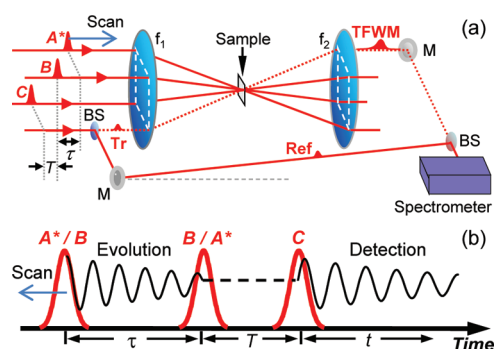


**Figure 2.** (a) The 2DFT spectroscopy setup, with notation.  $f_i$ , lens; BS, beam splitter; M, mirror; ref, reference pulse; Tr, tracer pulse. Scanning pulse  $A^*$  gives the  $S_I(\omega_n T, \omega_t)$  repasing spectrum. (b) Excitation sequence for the  $S_I(\omega_n T, \omega_t)$  repasing and  $S_{II}(\omega_n T, \omega_t)$  nonrepasing spectra.

In this paper, we study a GaAs QW sample using optical 2DFT spectroscopy. Homogeneous and inhomogeneous line widths for the intra-action  $X_{hh}$  and  $X_{lh}$  resonances are extracted.<sup>44</sup> We discuss the difference in the broadening mechanisms of the two excitons, namely the dominance of inhomogeneous broadening for the  $X_{hh}$  and homogeneous broadening for the  $X_{lh}$ . Results are presented for a range of excitation densities in the  $\chi^{(3)}$  regime, which also reveal excitation-induced dephasing and invariant disorder-induced broadening.

## EXPERIMENTS

A schematic diagram of the experimental setup is shown in Figure 2a. A mode-locked Ti:sapphire laser is the light source, producing <200 fs pulses, centered around 800 nm. The pulses are split into four replicas by a versatile ultrastable platform containing nested, phase-stabilized, and folded interferometers.<sup>45</sup> The platform generates the pulses in the box geometry, where the pulses propagate parallel to each other on the corners of a square in a plane transverse to the propagation direction. Three pulses are focused by a single lens to impinge the sample at the focus, where they overlap with  $1/e$  beam diameters of  $\sim 80 \mu\text{m}$ . These excitation pulses generated a TFWM signal in the appropriate phase-matching direction corresponding to the fourth corner of the square after recollimation by a lens. The fourth pulse traces out the direction of the signal, useful for alignment, but it is blocked during a 2DFT scan and is instead routed around the sample to be a reference pulse that is recombined with the collimated TFWM signal. The phase-stabilized reference pulse (local oscillator) is then used for heterodyne detection by spectral interferometry.<sup>46</sup> The spectral resolution of the apparatus is about  $40 \mu\text{eV}$ , which is determined by the resolution of the spectrometer used to produce the interferograms. This system is capable of capturing phase-resolved 2DFT spectra,<sup>40</sup> although we only present and discuss magnitude spectra in this paper.

The experimental geometry has three time periods:  $\tau$  between the first and second pulses,  $T$  between the second and third pulses, and  $t$  between the third pulse and the TFWM emission; see Figure 2b. For all the measurements presented in this paper,  $T$  is fixed at 200 fs.  $S_I(\omega_n T, \omega_t)$  spectra have the 2DFT taken with respect to the first and third time periods  $\tau$  and  $t$ , measured with the phase-matching condition  $k_I = -k_A + k_B + k_C$  while scanning pulse  $A^*$  earlier in time. These spectra are known as repasing, because effects of inhomogeneous broadening are canceled and the corresponding time-resolved TFWM signal exhibits a photon echo. In repasing spectra, the diagonal (equi-absorption-emission frequency line) has a

negative slope because the emission frequency is used to determine the arithmetic sign of the axes and the conjugate pulse is first in this pulse sequence, resulting in a negative sign for the Fourier-transformed frequency,  $\omega_\tau$ .

In  $S_{\text{I}}(\omega_\tau, T, \omega_t)$  spectra, the time order of the first two pulses is switched, such that pulse B is scanned earlier in time and the phase-matching condition becomes  $k_{\text{II}} = +k_{\text{A}} - k_{\text{B}} + k_{\text{C}}$ ; see Figure 2b. This excitation sequence does not produce a photon echo and is known as nonrephasing. Although no examples of these spectra are shown in this paper, they have references made to them.

The sample under investigation is an epitaxially grown, four-period GaAs multiple-QW with  $\text{Al}_{0.3}\text{Ga}_{0.7}\text{As}$  barriers; both wells and barriers are 10 nm thick. The sample is mounted on a sapphire plate and the substrate was removed for transmission measurements, which are performed at a temperature of approximately 6 K. The linear absorbance spectrum is presented in Figure 1c. The  $X_{\text{hh}}$  and  $X_{\text{lh}}$  peaks are separated by 8 meV and are excited simultaneously by the laser pulse spectrum, which is also shown. The polarization of the excitation beams is set to circular ( $\sigma^+$ ). Hence,  $\sigma^-$  transitions represented by dashed lines in Figure 1b are not accessible. For cocircular polarized ( $\sigma^+ \sigma^+ \sigma^+ \sigma^+$ ) = (representing the polarization of pulse A\*, B, C and the signal) 2DFT spectra, bound biexcitons do not contribute to the third-order signal,<sup>39</sup> and consequently are not discussed here. For this polarization mixed biexcitons are allowed;<sup>47</sup> however they are not observed, nor discussed.

## LINE WIDTH EXTRACTION

Multidimensional nuclear magnetic resonance spectroscopy focuses on peak strengths to extract coupling information and mostly ignores information in the two-dimensional line shape, beyond correcting phase twists and determining peak amplitudes.<sup>30</sup> In two-dimensional infrared spectroscopy, homogeneous and inhomogeneous line shapes have been considered in molecules.<sup>48</sup> The line widths of inhomogeneously broadened resonances in the diagonal and cross-diagonal directions of a rephasing  $S_{\text{I}}(\omega_\tau, T, \omega_t)$  2DFT spectrum are significantly different. Inhomogeneous broadening results in elongation along the diagonal line of a rephasing 2DFT spectrum. It is therefore possible to extract both the homogeneous line width ( $\gamma$ ) and inhomogeneous line width ( $\delta\omega$ ) from a single  $S_{\text{I}}(\omega_\tau, T, \omega_t)$  spectrum. Diagonal and cross-diagonal slices in the rephasing 2DFT spectra can be analyzed<sup>49</sup> by applying the projection-slice theorem<sup>30</sup> to the two-dimensional time data. The projection-slice theorem relates a projection in one domain of a multi-dimensional Fourier transform to a slice in the other dimension. Tokmakoff used this method to extract  $\gamma$  and  $\delta\omega$  for two extreme cases,<sup>49</sup> (a) for a purely homogeneous line shape ( $\delta\omega = 0$ ) and (b) for a strongly inhomogeneous line shape ( $\delta\omega \gg \gamma$ ).

For excitonic resonances in semiconductors, the weak inhomogeneous regime ( $\delta\omega \approx \gamma$ ) is also of importance, as observed in the rephasing optical 2DFT spectrum shown in Figure 3. Recently methods have been proposed to relate theoretical values of  $\gamma$  and  $\delta\omega$  to the line shapes found in experiments. In one method, the peak-to-peak distances along the dispersive directions of phase-resolved rephasing (R) and nonrephasing (NR) spectra are extracted.<sup>6</sup> The extracted value  $\Delta\Omega_{\text{R}}$  is proportional to  $\gamma$ . The value from the nonrephasing spectrum  $\Delta\Omega_{\text{NR}}$  contains contributions from the pure inhomogeneous and homogeneous broadening, such that  $\Delta\Omega_{\text{NR}} - \Delta\Omega_{\text{R}} = \Delta\Omega_{\text{NR-R}}$  is proportional to  $\delta\omega$ . This method was determined to account for many-body interactions of semiconductor excitons. Model calculations show that  $\Delta\Omega_{\text{R}} \approx 0.9 \times \gamma$ , whereas  $\Delta\Omega_{\text{NR-R}}$  is approximately equal to the inhomogeneous width.<sup>50</sup>

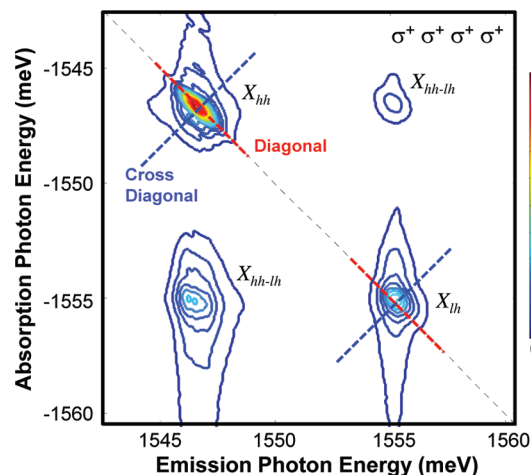


**Figure 3.** Rephasing  $|S_{\text{I}}(\omega_\tau, T, \omega_t)|$  spectrum for the GaAs QW excited with cocircular ( $\sigma^+ \sigma^+ \sigma^+ \sigma^+$ ) polarization. Dashed lines indicate the diagonal and cross-diagonal slices for  $X_{\text{hh}}$  and  $X_{\text{lh}}$ .

A second method of relating the observed line shape to  $\gamma$  and  $\delta\omega$  extends the treatment of the time-domain signal analysis developed by Tokmakoff.<sup>49</sup> Starting with a simulation of the optical Bloch equations for the TFWM signal in the time domain, analytical expressions for the calculated signal can be manipulated using the slice-projection theorem rather than performing the usual 2DFT.<sup>44</sup> The diagonal of the two-dimensional time map is dominated by dephasing for both homogeneously and inhomogeneously broadened spectra. Projection of the time data onto the diagonal yields a one-dimensional function that will mostly represent the homogeneous dephasing but will be modified by the inhomogeneous dephasing. Similarly, a projection of the time data onto a line through the origin in a direction perpendicular to the diagonal gives a function that is strongly dominated by inhomogeneous dephasing. Fourier-transforming these one-dimensional projections yields slices in the 2DFT spectra that correspond to the diagonal ( $\omega_\tau$ ) and cross-diagonal ( $\omega_\tau'$ ) directions, with some appropriate frequency offset. These directions are represented by dashed lines over the  $X_{\text{hh}}$  and  $X_{\text{lh}}$  intra-action resonances in Figure 3. The functional forms of these slices can then be used to fit the diagonal and cross-diagonal slices of a rephasing 2DFT spectrum. Complete details of this analysis is given in Siemens et al.<sup>44</sup>

In the limit of weak inhomogeneous broadening,  $\gamma$  and  $\delta\omega$  contribute to both the diagonal and cross-diagonal slices of the 2DFT line shape. The functional forms for line shape slices with arbitrary Gaussian inhomogeneity and assuming Lorentzian homogeneous broadening are

$$S(\omega_\tau) = \frac{\exp\left\{\frac{(\gamma - i\omega_\tau)^2}{2\delta\omega^2}\right\} \left( \text{Erfc}\left[\frac{\gamma - i\omega_\tau}{\sqrt{2}\delta\omega}\right] + \exp\left\{\frac{2i\gamma\omega_\tau}{\delta\omega^2}\right\} \text{Erfc}\left[\frac{\gamma + i\omega_\tau}{\sqrt{2}\delta\omega}\right] \right)}{\gamma\delta\omega\sqrt{\frac{2}{\pi}}} \quad (1)$$

$$S(\omega_\tau') = \frac{\exp\left\{\frac{(\gamma - i\omega_\tau')^2}{2\delta\omega^2}\right\} \text{Erfc}\left\{\frac{\gamma - i\omega_\tau'}{\sqrt{2}\delta\omega}\right\}}{\delta\omega(\gamma - i\omega_\tau')} \quad (2)$$



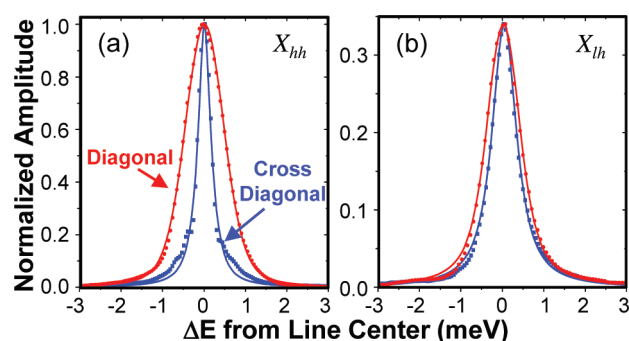


**Figure 4.** Diagonal (red circles) and cross-diagonal (blue squares) data slices along with their respective fits (lines) for the (a)  $X_{hh}$  and (b)  $X_{lh}$  resonances.

where  $\text{Erfc}(x)$  is the complex complementary error function. These expressions are for the complex projection, thus real imaginary or amplitude line shapes can be fit. Here we chose to fit the amplitude  $|S(\omega_i)|$ , where  $i = \tau', l'$ .

Figure 4 shows the diagonal and cross-diagonal data slices and fits using eqs 1 and 2. The excellent fits show that Gaussian inhomogeneity and Lorentzian homogeneous broadening are reasonable assumptions for the level of disorder present in this well.<sup>51</sup> The two slices can be fit simultaneously to obtain consistent values. Additionally, this analysis can be extended to find functional forms for slices in the nonrephasing spectrum. However, these fits are not as robust and do not provide any additional information, since the nonrephasing is formally identical to a one-dimensional scan. Including phenomenological many-body terms in the optical Bloch equations does not result in a significant change in the extracted linewidths.

## RESULTS AND DISCUSSION

As discussed elsewhere,<sup>29</sup> the important characteristics of the 2DFT spectra in Figure 3 are diagonal intra-action resonances of the two exciton species, two off-diagonal interaction resonances, and vertical stripes associated with excitation of  $e-hh$  continuum states. In phase-resolved 2DFT spectra (not shown here) the line shapes of most features are dispersive, resulting from many-body interactions, particularly excitation-induced shifts<sup>33</sup> in a phenomenological description. Qualitatively, these spectra match well to microscopic one-dimensional tight-binding calculations, which include Coulomb correlations beyond the Hartree–Fock mean-field approximation<sup>38</sup> and phenomenological Gaussian inhomogeneous broadening.<sup>6</sup> More recently, the inhomogeneous broadening has been modeled with multiple realizations of fluctuating energy levels to simulate structural disorder, a more realistic microscopic picture, and has again shown good qualitative agreement with experimental spectra.<sup>52</sup>

It should be noted that the data presented here has finer resolution than that used in previous experiment-to-theory comparisons of the homogeneous and inhomogeneous line widths.<sup>52,53</sup> This difference hinders direct comparison between those studies and the work presented here. The values for  $\gamma$  and  $\delta\omega$  obtained from fitting rephasing data slices in Figure 4a,b are shown in Table 1. These values are used to simulate the 2DFT spectrum for comparison. Figure 5 shows the numerical simulation, which is performed using the optical Bloch equations for a closed three-level system.<sup>54</sup> The excitation is introduced as  $\delta$ -function pulses and many-body interactions are excluded, so

**Table 1.** Bulk Values for Hole Mass ( $m_h^*$ ), Reduced Mass ( $\mu$ ), Exciton Bohr Radius ( $a_X$ ) and Extracted Homogeneous ( $\gamma$ ) and Inhomogeneous ( $\delta\omega$ ) Line Widths for Heavy-Hole and Light-Hole Excitons

	$m_h^* (m_e)$	$\mu (m_e)$	$a_X (\text{nm})$	$\gamma (\text{meV})$	$\delta\omega (\text{meV})$
$X_{hh}$	0.473	0.0556	6.30	0.13	0.40
$X_{lh}$	0.082	0.0353	9.93	0.30	0.26

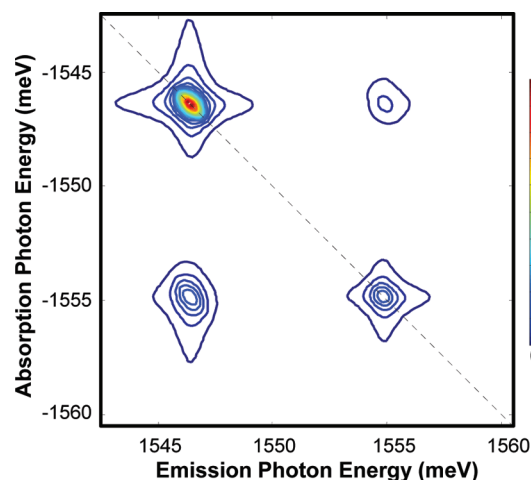


**Figure 5.** (a) Simulation of rephasing  $|S_I(\omega_\tau, T, \omega_l)|$  spectrum for the GaAs QW using optical Bloch equations with line widths extracted from the diagonal and cross-diagonal data slices for each resonance.

the peak amplitudes have been adjusted manually to account for the spectral weighting due to finite duration pulses. This phenomenological model qualitatively replicates the experimental two-dimensional spectral line shapes of the excitonic resonances. The vertical features present in the experimental data are due to many-body interactions with unbound electron–hole pairs,<sup>32</sup> which are not included in the model.

The most striking feature in the 2DFT spectrum is the difference in the two-dimensional line shapes of the  $X_{hh}$  and  $X_{lh}$ . Elongated along the diagonal, the  $X_{hh}$  is dominated by inhomogeneous broadening (approximately three times larger than the homogeneous broadening). In comparison, the  $X_{lh}$  has a larger homogeneous width than the  $X_{hh}$  due to spectral overlap and coupling between the bound  $e-lh$  excitons to the  $e-hh$  continuum states, which are known to have a faster dephasing rate.<sup>55,56</sup> This quantum mechanical coupling leads to dephasing, but does not produce a Fano line shape in the 2DFT spectra.<sup>52,57</sup> On the other hand, the  $X_{lh}$  has a smaller inhomogeneous width than the  $X_{hh}$ , such that the diagonal and cross-diagonal line widths of the  $X_{lh}$  are similar. Analysis using the peak-to-peak distances in dispersive spectra also concluded that the  $X_{lh}$  has a smaller inhomogeneous width than the  $X_{hh}$ .<sup>50</sup> This difference means that while the  $X_{hh}$  is strongly dominated by disorder, the  $X_{lh}$  is not.

The sizable difference in the  $X_{hh}$  and  $X_{lh}$  inhomogeneous line widths is initially surprising, but Kuznetsova et al. found that this difference can be explained in terms of the Bohr radii ( $a_X$ ) of the respective excitons and the length scale of the disorder potential ( $l_d$ ) in the QW.<sup>52</sup> When  $a_X \gg l_d$ , the exciton center-of-mass motion averages over the disorder, whereas if  $a_X \ll l_d$  there are no fluctuations for the exciton to sense. Between these extremes, when  $l_d$  is close to  $a_X$  and the excitonic localization length, the

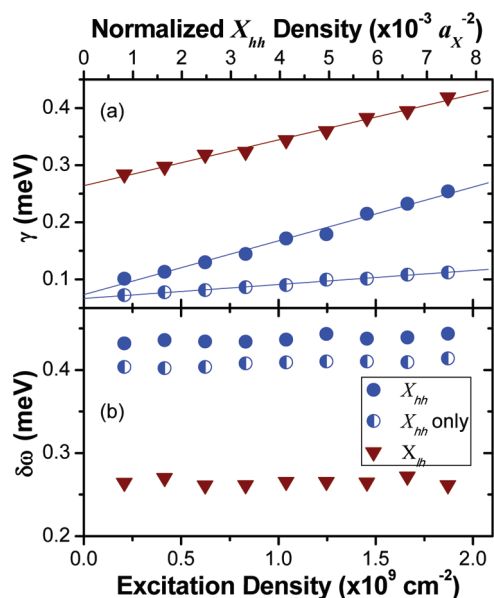


**Figure 6.** Excitation-density dependence of the (a) homogeneous and (b) pure inhomogeneous line widths extracted from the repurposing 2DFT spectra for both exciton species and for the  $X_{hh}$  when excited alone. Solid lines are linear fits for the excitation-induced homogeneous line width change.

exciton is the most sensitive to the disorder.<sup>58</sup> The two-dimensional exciton Bohr radius is

$$a_X = \frac{\hbar^2 \epsilon_0}{2\mu e^2} \quad (3)$$

and is half the value for excitons in bulk.<sup>59</sup> Since  $\hbar$ ,  $\epsilon_0$ , and  $e$  are physical constants, the only difference between the two exciton species is the reduced excitonic mass, which is

$$\mu = \frac{m_e^* m_v^*}{m_e^* + m_v^*} \quad (4)$$

The effective mass of the electron ( $m_e^*$ ) is the same for both excitons, but the effective mass of the valence bands ( $m_v^*$ ) differ. Bulk values for  $m_v^*$ ,  $\mu$ , and  $a_X$  are shown in Table 1. The valence band effective masses will be modified by quantum confinement in a heterostructure and strain.<sup>60</sup> Because these effects depend sensitively on the exact structure and strain, which may vary from sample-to-sample due to mounting and etching, we will simply use the bulk values as a reasonable estimate. Since the disorder is determined in the growth process then for this sample it seems reasonable to conclude that the length scale of the disorder is larger for length scales close to the  $X_{hh}$  Bohr radius of  $\sim 6$  nm than for the  $X_{lh}$  Bohr radius. However, theory suggests that some of the reduction of the inhomogeneous broadening of the  $X_{lh}$  may be due to coupling to the hh-continuum states.<sup>52</sup> This result invites a systematic study of disorder-induced broadening and the exciton localization parameters by 2DFT spectroscopy for QWs with variation in growth interruption times.<sup>61–65</sup>

Disorder-induced and other broadening mechanisms are clearly separated by 2DFT spectroscopy. The excitation-induced dephasing contribution to the coherent response can be determined from the variation of the homogeneous line width in excitation-density-dependent measurements, performed in the  $\chi^{(3)}$  regime.<sup>11,12,66</sup> Figure 6 shows the extracted (a) homogeneous and (b) inhomogeneous line widths as a function of

excitation power of the  $X_{hh}$  and  $X_{lh}$  when the laser has sufficient bandwidth to excite both resonances simultaneously. From these data, the line width at zero excitation density can be determined by extrapolation. Also shown are the line widths for the  $X_{hh}$  when excited alone by spectrally filtered laser pulses, denoted as  $X_{hh}$  only.

Over the range of excitation densities shown in Figure 6 the homogeneous line width increases by approximately 0.15 meV for  $X_{hh}$  and  $X_{lh}$ , that is, the two slopes are  $\sim 9 \times 10^{-11} \text{ meV/cm}^{-2}$ , as determined by a linear fit. The excitation density is estimated by measuring the fraction of the laser power that is absorbed and the spot size. The density is then calculated for an equivalent top hat profile. This approximation is reasonable since the signal is cubic in intensity, which strongly weights the center of the laser spot. Although the excitons have different energies and oscillator strengths, they both experience similar amounts of excitation-induced dephasing. However, the zero-excitation homogeneous line widths differ; extrapolated values are  $\gamma_{0,hh} = 0.073 \pm 0.005 \text{ meV}$  and  $\gamma_{0,lh} = 0.26 \pm 0.003 \text{ meV}$ , which confirms that the  $X_{lh}$  has a larger natural homogeneous line width.

Experiments performed with spectrally filtered excitation pulses excite only the  $X_{hh}$  resonance, suppressing excitation of the e-hh continuum or  $X_{lh}$ . In the vicinity of the  $X_{hh}$  resonance, the filtered spectrum very closely matches the full spectrum (see Figure 1c for comparison of the two spectra). In this case, the slope of the homogeneous line width for the  $X_{hh}$  decreases to  $\sim 2 \times 10^{-11} \text{ meV/cm}^{-2}$ . However, the extrapolated natural homogeneous line width is unchanged within experimental errors. This difference in slopes demonstrates that exciton–exciton scattering and exciton-free-carrier scattering mechanisms significantly contribute to the excitation-induced dephasing of the  $X_{hh}$  resonance.<sup>55</sup>

The inhomogeneous width of both resonances is essentially independent of excitation density. This result is not surprising as the inhomogeneity arises primarily from structural disorder, which should not be sensitive to excitation density. There does appear to be a slight reduction in the inhomogeneous width of the  $X_{hh}$  resonance when only  $X_{hh}$  is excited as compared to broadband excitation. Most likely this result is an artifact due to weighting of the 2DFT spectrum by the laser spectrum.

## CONCLUSION

In summary, we have explored the  $X_{hh}$  and  $X_{lh}$  resonances in GaAs QWs using 2DFT spectroscopy to isolate the pure inhomogeneous and homogeneous line widths. In GaAs QWs, we determine the different spectral broadening mechanism for the two species of exciton, which reflect the microscopic disorder and the localization lengths that the excitons experience. Disorder is affected by the growth conditions; in these high-quality molecular beam epitaxy samples, the  $X_{hh}$  resonance exhibits more inhomogeneous broadening than the  $X_{lh}$  resonance and hence is more sensitive to the length scale of the disorder. This finding suggests that 2DFT spectroscopy can determine the relationship between QW growth and the resulting exciton localization and should be used to perform a broader study. The migration of excitons among localization sites<sup>67</sup> can also be studied by collecting 2DFT spectra as a function of  $T$ . Such a study would help explain the observation of non-Markovian dynamics using three-pulse echo peak shift spectroscopy.<sup>68</sup>

We also separate the disorder-induced and excitation-induced broadening. We observe that the disorder-induced broadening

does not change over the excitation range presented, while the excitation-induced dephasing increases. This result is not unexpected, although it is a benefit of 2DFT spectroscopy because these mechanisms are often inseparable in other experimental techniques. This ability represents a step toward using 2DFT spectroscopy to find correlation lengths of many-body interactions in disorder solid-state systems.

## AUTHOR INFORMATION

### Corresponding Author

\*E-mail: cundiff@jila.colorado.edu.

### Present Addresses

<sup>||</sup>Department of Physics, West Virginia University, Morgantown, WV 26506–6315.

<sup>⊥</sup>College of Nanoscale Science and Engineering, State University of New York at Albany, Albany, NY 12203.

<sup>†</sup>Department of Physics and Astronomy, University of Denver, Denver, CO 80208–0183.

## ACKNOWLEDGMENT

The authors wish to thank Torsten Meier and Peter Thomas for useful discussions. This work was supported by the National Science Foundation and the Chemical Sciences, Geosciences, and Biosciences Division Office of Basic Energy Sciences, U.S. Department of Energy and by the National Science Foundation.

## REFERENCES

- (1) Klingshirn, C. F. *Semiconductor Optics*; Springer-Verlag: Berlin, 2007.
- (2) Skolnick, M. S.; Tapster, P. R.; Bass, S. J.; Pitt, A. D.; Apsley, N.; Aldred, S. P. *Semicon. Sci. Technol.* **1986**, *1*, 29–40.
- (3) Ferreira, R.; Bastard, G. *Phys. Rev. B* **1991**, *43*, 9687–9691.
- (4) Axt, V. M.; Kuhn, T. *Rep. Prog. Phys.* **2004**, *67*, 433–512.
- (5) Cundiff, S. T. *Opt. Express* **2008**, *16*, 4639–4664.
- (6) Kuznetsova, I.; Meier, T.; Cundiff, S. T.; Thomas, P. *Phys. Rev. B* **2007**, *76*, 153301.
- (7) Göbel, E. O.; Leo, K.; Damen, T. C.; Shah, J.; Schmitt-Rink, S.; Schäfer, W.; Müller, J. F.; Köhler, K. *Phys. Rev. Lett.* **1990**, *64*, 1801–1804.
- (8) Chemla, D. S.; Shah, J. *Nat.* **2001**, *411*, 549–557.
- (9) Leo, K.; Wegener, M.; Shah, J.; Chemla, D. S.; Göbel, E. O.; Damen, T. C.; Schmitt-Rink, S.; Schäfer, W. *Phys. Rev. Lett.* **1990**, *65*, 1340–1343.
- (10) Kuklinski, J. R.; Mukamel, S. *Phys. Rev. B* **1991**, *44*, 11253–11259.
- (11) Wang, H. L.; Ferrio, K.; Steel, D. G.; Hu, Y. Z.; Binder, R.; Koch, S. W. *Phys. Rev. Lett.* **1993**, *71*, 1261–1264.
- (12) Hu, Y. Z.; Binder, R.; Koch, S. W.; Cundiff, S. T.; Wang, H.; Steel, D. G. *Phys. Rev. B* **1994**, *49*, 14382–14386.
- (13) Bott, K.; Heller, O.; Bennhardt, D.; Cundiff, S. T.; Thomas, P.; Mayer, E. J.; Smith, G. O.; Eccleston, R.; Kuhl, J.; Ploog, K. *Phys. Rev. B* **1993**, *48*, 17418–17426.
- (14) Smirl, A. L.; Stevens, M. J.; Chen, X.; Buccafusca, O. *Phys. Rev. B* **1999**, *60*, 8267–8275.
- (15) Wachter, S.; Maute, M.; Kalt, H.; Galbraith, I.; Sieh, C.; Meier, T.; Koch, S. W. *Phys. B* **2002**, *314*, 309–313.
- (16) Shacklette, J. M.; Cundiff, S. T. *Phys. Rev. B* **2002**, *66*, 045309.
- (17) Mayer, E. J.; Smith, G. O.; Heuckeroth, V.; Kuhl, J.; Bott, K.; Schulze, A.; Meier, T.; Bennhardt, D.; Koch, S. W.; Thomas, P.; Hey, R.; Ploog, K. *Phys. Rev. B* **1994**, *50*, 14730–14733.
- (18) Saiki, T.; Kuwatagonokami, M.; Matsusue, T.; Sakaki, H. *Phys. Rev. B* **1994**, *49*, 7817–7820.
- (19) Adachi, S.; Miyashita, T.; Takeyama, S.; Takagi, Y.; Takeuchi, A.; Nakayama, M. *Phys. Rev. B* **1997**, *55*, 1654–1660.
- (20) Cundiff, S. T.; Wang, H.; Steel, D. G. *Phys. Rev. B* **1992**, *46*, 7248–7251.
- (21) Schmitt-Rink, S.; Bennhardt, D.; Heuckeroth, V.; Thomas, P.; Haring, P.; Maidorn, G.; Bakker, H.; Leo, K.; Kim, D. S.; Shah, J.; Köhler, K. *Phys. Rev. B* **1992**, *46*, 10460–10463.
- (22) Weiser, S.; Meier, T.; Mobius, J.; Euteneuer, A.; Mayer, E. J.; Stolz, W.; Hofmann, M.; Ruhle, W. W.; Thomas, P.; Koch, S. W. *Phys. Rev. B* **2000**, *61*, 13088–13098.
- (23) Albrecht, T. F.; Bott, K.; Meier, T.; Schulze, A.; Koch, M.; Cundiff, S. T.; Feldmann, J.; Stolz, W.; Thomas, P.; Koch, S. W.; Göbel, E. O. *Phys. Rev. B* **1996**, *54*, 4436–4439.
- (24) Langbein, W.; Hvam, J. M.; Umlauff, M.; Kalt, H.; Jobst, B.; Hommel, D. *Phys. Rev. B* **1997**, *55*, R7383–R7386.
- (25) Langbein, W.; Hvam, J. M.; Zimmermann, R. *Phys. Rev. Lett.* **1999**, *82*, 1040–1043.
- (26) Mukamel, S. *Annu. Rev. Phys. Chem.* **2000**, *51*, 691–729.
- (27) Jonas, D. *Annu. Rev. Phys. Chem.* **2003**, *54*, 425–463.
- (28) Cho, M. *Chem. Rev.* **2008**, *108*, 1331–1418.
- (29) Cundiff, S. T.; Zhang, T.; Bristow, A. D.; Karauskaj, D.; Dai, X. *Acc. Chem. Res.* **2009**, *42*, 1423–1432.
- (30) Ernst, R.; Bodenhausen, G.; Wokaun, A. *Principles of Nuclear Magnetic Resonance in One and Two Dimensions*; Oxford Science Publications: Oxford, 1987.
- (31) Tanimura, Y.; Mukamel, S. *J. Chem. Phys.* **1993**, *99*, 9496–9511.
- (32) Borca, C. N.; Zhang, T. H.; Li, X. Q.; Cundiff, S. T. *Chem. Phys. Lett.* **2005**, *416*, 311–315.
- (33) Li, X. Q.; Zhang, T. H.; Borca, C. N.; Cundiff, S. T. *Phys. Rev. Lett.* **2006**, *96*, 057406.
- (34) Yang, L.; Mukamel, S. *Phys. Rev. Lett.* **2008**, *100*, 057402.
- (35) Stone, K. W.; Gundogdu, K.; Turner, D. B.; Li, X.; Cundiff, S. T.; Nelson, K. A. *Science* **2009**, *324*, 1169–1173.
- (36) Karauskaj, D.; Bristow, A. D.; Yang, L.; Dai, X.; Mirin, R. P.; Mukamel, S.; Cundiff, S. T. *Phys. Rev. Lett.* **2010**, *104*, 117401.
- (37) Yang, L. J.; Schweigert, I. V.; Cundiff, S. T.; Mukamel, S. *Phys. Rev. B* **2007**, *75*, 125302.
- (38) Zhang, T.; Kuznetsova, I.; Meier, T.; Li, X.; Mirin, R. P.; Thomas, P.; Cundiff, S. T. *Proc. Nat. Acad. Sci. U.S.A.* **2007**, *104*, 14227–14232.
- (39) Bristow, A. D.; Karauskaj, D.; Dai, X.; Mirin, R. P.; Cundiff, S. T. *Phys. Rev. B* **2009**, *79*.
- (40) Bristow, A. D.; Karauskaj, D.; Dai, X.; Cundiff, S. T. *Opt. Express* **2008**, *16*, 18017–18027.
- (41) Langbein, W.; Patton, B. *Opt. Lett.* **2006**, *31*, 1151–1153.
- (42) Brixner, T.; Stenger, J.; Vaswani, H.; Cho, M.; Blankenship, R.; Fleming, G. *Nature* **2005**, *434*, 625–628.
- (43) Engel, G. S.; Calhoun, T. R.; Read, E. L.; Ahn, T.-K.; Mancal, T.; Cheng, Y.-C.; Blankenship, R. E.; Fleming, G. R. *Nature* **2007**, *446*, 782–786.
- (44) Siemens, M. E.; Moody, G.; Li, H.; Bristow, A. D.; Cundiff, S. T. *Opt. Express* **2010**, *18*, 17699–17708.
- (45) Bristow, A. D.; Karauskaj, D.; Dai, X.; Zhang, T.; Carlsson, C.; Hagen, K. R.; Jimenez, R.; Cundiff, S. T. *Rev. Sci. Instrum.* **2009**, *80*, 073108.
- (46) Lepetit, L.; Cheriaux, G.; Joffre, M. J. *Opt. Soc. Am. B* **1995**, *12*, 2467–2474.
- (47) Wagner, H. P.; Langbein, W.; Hvam, J. M. *Phys. Rev. B* **1999**, *59*, 4584–4587.
- (48) Faeder, S. M. G.; Jonas, D. M. *J. Phys. Chem. A* **1999**, *103*, 10489–10505.
- (49) Tokmakoff, A. *J. Phys. Chem. A* **2000**, *104*, 4247–4255.
- (50) Kuznetsova, I.; Thomas, P.; Meier, T.; Zhang, T.; Cundiff, S. T. *Phys. Status Solidi C* **2009**, *6*, 445–448.
- (51) Schnabel, R. F.; Zimmermann, R.; Bimberg, D.; Nickel, H.; Lösch, R.; Schlapp, W. *Phys. Rev. B* **1992**, *46*, 9873–9876.
- (52) Kuznetsova, I.; Gogh, N.; Forstner, J.; Meier, T.; Cundiff, S. T.; Varga, I.; Thomas, P. *Phys. Rev. B* **2010**, *81*, 075307.

- (53) Kuznetsova, I.; Thomas, P.; Meier, T.; Zhang, T.; Li, X.; Mirin, R. P.; Cundiff, S. T. *Solid State Commun.* **2007**, *142*, 154–158.
- (54) Yajima, T.; Taira, Y. *J. Phys. Soc. Japan* **1979**, *47*, 1620–1626.
- (55) Honold, A.; Schultheis, L.; Kuhl, J.; Tu, C. W. *Phys. Rev. B* **1989**, *40*, 6442–6445.
- (56) Gopal, A. V.; Vengurlekar, A. S. *Phys. Rev. B* **2000**, *62*, 4624–4629.
- (57) Pasquarello, A.; Andreani, L. C. *Phys. Rev. B* **1991**, *44*, 3162–3167.
- (58) Baranovskii, S. D.; Efros, A. L. *Soviet Phys. Semicon.* **1978**, *12*, 1328–1330.
- (59) Haug, H.; Koch, S. *Quantum Theory of the Optical and Electronic Properties of Semiconductors*, 5th ed.; World Scientific Publishing Company: Singapore, 2009.
- (60) Bastard, G.; Brum, J. *IEEE J. Quantum Electron.* **1986**, *22*, 1625–1644.
- (61) Miller, R. C.; Tu, C. W.; Sputz, S. K.; Kopf, R. F. *Appl. Phys. Lett.* **1986**, *49*, 1245–1247.
- (62) Tanaka, M.; Sakaki, H.; Yoshino, J. *Jpn. J. Appl. Phys., Part 2* **1986**, *25*, L155–L158.
- (63) Shimomura, S.; Wakejima, A.; Adachi, A.; Okamoto, Y.; Sano, N.; Murase, K.; Hiyamizu, S. *Jpn. J. Appl. Phys.* **1993**, *32*, L1728–L1731.
- (64) Leosson, K.; Jensen, J. R.; Langbein, W.; Hvam, J. M. *Phys. Rev. B* **2000**, *61*, 10322–10329.
- (65) Savona, V.; Langbein, W. *Phys. Rev. B* **2006**, *74*, 075311.
- (66) Schultheis, L.; Kuhl, J.; Honold, A.; Tu, C. W. *Phys. Rev. Lett.* **1986**, *57*, 1635–1638.
- (67) Webb, M. D.; Cundiff, S. T.; Steel, D. G. *Phys. Rev. B* **1991**, *43*, 12658–12661.
- (68) Carter, S. G.; Chen, Z.; Cundiff, S. T. *Phys. Rev. B* **2007**, *76*, 121303.